

# Sat3R: Satellite DSM Reconstruction via RPC-Aware Depth Fine-tuning

Qiaoyi Yang<sup>1</sup>, Chaoyi Zhou<sup>1</sup>, Xi Liu<sup>1</sup>, Run Wang<sup>1</sup>, Minghui Xu<sup>1</sup>, Mert D. Pesé<sup>1</sup>  
Feng Luo<sup>1</sup>, Yuhao Xu<sup>1</sup>, Zhi-Qi Cheng<sup>2</sup>, Qiushi Chen<sup>1</sup>, Hairong Qi<sup>3</sup>, Siyu Huang<sup>1</sup>

<sup>1</sup>Clemson University

<sup>2</sup>University of Washington

<sup>3</sup>University of Tennessee

## Abstract

Accurate Digital Surface Model (DSM) reconstruction from satellite imagery is critical for applications such as disaster response, urban planning, and large-scale geographic mapping. Existing approaches face a fundamental trade-off: optimization-based methods achieve strong accuracy but require hours of per-scene computation, while generalizable geometry foundation models offer near-instant inference but fail to generalize to satellite imagery due to the domain gap introduced by the Rational Polynomial Camera (RPC) model and mismatched depth scale distributions. We present Sat3R, a feed-forward framework that bridges this gap via RPC-aware metric depth fine-tuning of Depth Anything V2 using the Scale-Invariant Logarithmic (SiLog) loss. By constructing physically consistent pseudo depth supervision from RPC geometry, Sat3R adapts a monocular depth foundation model to the satellite domain without per-scene optimization. Experiments on the DFC2019 benchmark demonstrate that Sat3R reduces MAE by 38% over zero-shot feed-forward baselines and achieves competitive accuracy against optimization-based methods, while delivering over 300× speedup. Sat3R demonstrates that feed-forward models, when properly adapted to the satellite domain, can match optimization-based accuracy at a fraction of the computational cost, paving the way for practical large-scale satellite DSM reconstruction.

## 1. Introduction

Accurate Digital Surface Model (DSM) reconstruction from satellite imagery supports a wide range of applications, including disaster response, urban planning, and large-scale geographic mapping. Given multi-view satellite images and their associated Rational Polynomial Camera (RPC) metadata, the goal is to recover a dense height map of the observed scene.

Existing approaches fall into two categories. Optimization-based methods such as SatDN [8] achieve competitive DSM accuracy by fitting a neural representa-

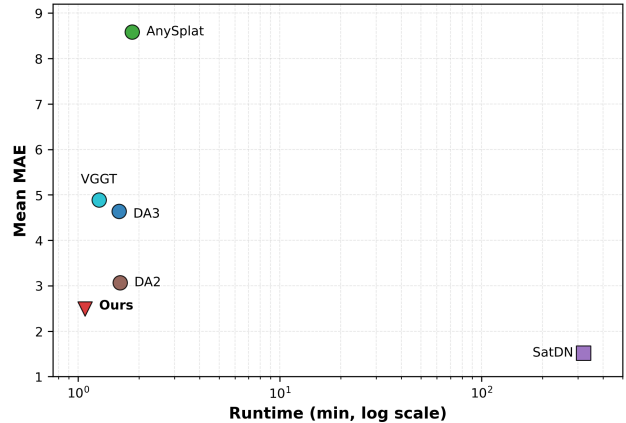


Figure 1. Runtime vs. accuracy comparison on DFC2019 [17]. Sat3R is the first feed-forward framework for satellite DSM reconstruction, achieving comparable accuracy to optimization-based SatDN with over 300× speedup, while outperforming all zero-shot feed-forward baselines in reconstruction accuracy.

tion per scene, but require hours of optimization per scene, making them impractical for time-sensitive applications. On the other hand, generalizable geometry foundation models (GFMs) [21, 28] offer near-instant inference without per-scene optimization, but perform poorly when applied directly to satellite imagery. As shown in Fig. 1, optimization-based methods achieve strong accuracy but at the cost of hours of computation per scene, while GFMs offer near-instant inference but with substantially degraded accuracy on satellite imagery — no existing method delivers both the speed required for operational deployment and the accuracy demanded by downstream applications.

We identify two key reasons for this failure of GFMs on satellite data. First, satellite cameras follow the Rational Polynomial Camera (RPC) model, which has no explicit camera center, making the physical definition of depth fundamentally incompatible with the perspective-camera assumption underlying these models. Second, the depth scale distribution of satellite imagery differs substantially from the natural image datasets on which these models are trained.

To bridge this domain gap, we propose **Sat3R**, an RPC-aware fine-tuning approach. We construct image–depth training pairs from the training split of the DFC2019 satellite dataset [17] by defining a physically consistent pseudo depth based on RPC geometry: for each pixel, we compute the slant-range distance between a near-plane reference point and the true surface intersection along the imaging ray. This pseudo depth serves as metric depth supervision to fine-tune Depth Anything V2 (DA2) [28] using the Scale-Invariant Logarithmic (SiLog) loss [1]. At inference, predicted depths are back-projected through the RPC model to produce a DSM. As illustrated in Fig. 1, compared to zero-shot feed-forward baselines, our method reduces MAE by 38%. Compared to optimization-based SatDN, Sat3R achieves competitive accuracy while delivering over  $300\times$  speedup.

In summary, our contributions are:

- We propose **Sat3R**, the first feed-forward framework for satellite DSM reconstruction, enabling efficient inference without per-scene optimization.
- We introduce a pseudo depth construction pipeline for RPC satellite imagery, providing physically consistent metric depth supervision for fine-tuning monocular depth foundation models.
- Extensive experiments on the DFC2019 dataset demonstrate that Sat3R achieves competitive DSM accuracy against optimization-based methods with over  $300\times$  speedup, while outperforming all zero-shot feed-forward baselines by 38% in MAE.

## 2. Related Work

### 2.1. Optimization-Based 3D Reconstruction

Classical multi-view stereo (MVS) methods reconstruct 3D structure by matching correspondences across images and optimizing for geometric consistency [15, 18–20]. While effective, these pipelines require careful calibration and are computationally expensive at scale. Neural rendering approaches such as NeRF [12–14, 22] have significantly advanced reconstruction quality by representing scenes as continuous volumetric functions optimized per scene. More recent methods based on 3D Gaussian Splatting (3DGS) [3, 5, 9, 29, 31] improve rendering efficiency while maintaining competitive reconstruction quality. However, the per-scene optimization nature of these methods results in inference times on the order of minutes to hours, limiting their applicability in time-sensitive scenarios such as disaster response and large-scale mapping.

### 2.2. Generalizable Geometry Foundation Models

Recent work has demonstrated that large-scale pretraining can yield powerful geometry estimators [4, 6, 7, 21, 23–26, 28, 30, 32] that generalize across scenes without per-

scene optimization. For monocular depth estimation, Depth Anything (DA) [7, 27, 28] achieves strong zero-shot performance on natural images by training on large-scale labeled and unlabeled data. For multi-view geometry, models such as VGGT [21] and AnySplat [4] directly infer 3D structure from multiple input views in a single feed-forward pass. Despite their efficiency, these models are trained exclusively on natural image datasets and fail to generalize to satellite imagery, where the RPC camera model and depth scale distribution differ fundamentally from the perspective-camera assumption underlying these methods. This domain gap motivates our work, which constructs RPC-aware training data to adapt DA2 [28] for satellite DSM reconstruction.

### 2.3. Satellite 3D Reconstruction

Early attempts to apply neural rendering to satellite imagery adapt NeRF to the unique properties of satellite acquisition. Several works focus on appearance modeling, incorporating shadow cues [10], and dynamic object uncertainty [11] to improve novel view synthesis quality. Others target geometric accuracy, introducing photo-consistency constraints [16] or hash-grid representations [2] to accelerate optimization. SatDN [8] extends this line by adapting the RPC camera model into a NeRF-based framework, achieving strong DSM accuracy but requiring hours of per-scene optimization. Our work departs from this paradigm by adopting a feed-forward approach, eliminating per-scene optimization entirely.

## 3. Method

### 3.1. Problem Formulation

Given a set of  $N$  overlapping satellite images  $\{I_i\}_{i=1}^N$  and their associated RPC models  $\{R_i\}_{i=1}^N$ , our goal is to reconstruct a Digital Surface Model (DSM) representing the height of the scene at each geographic location. The overall pipeline of Sat3R is shown in Fig. 2.

### 3.2. Pseudo Depth Construction

Satellite imagery is governed by the RPC model, which provides no explicit camera center, making standard perspective depth undefined. We define a physically consistent pseudo depth analogous to the camera-to-surface distance in perspective geometry.

For each image, we define a near-plane at altitude:

$$z_{\text{ref}} = z_{\text{max}} + \delta \quad (1)$$

where  $z_{\text{max}}$  is the maximum scene altitude from image metadata and  $\delta = 50$  m is a fixed margin. For each pixel, we compute its RPC imaging ray and find its intersection with the near-plane  $\mathbf{p}_{\text{near}}$  and with the true surface  $\mathbf{p}_{\text{surface}}$  via

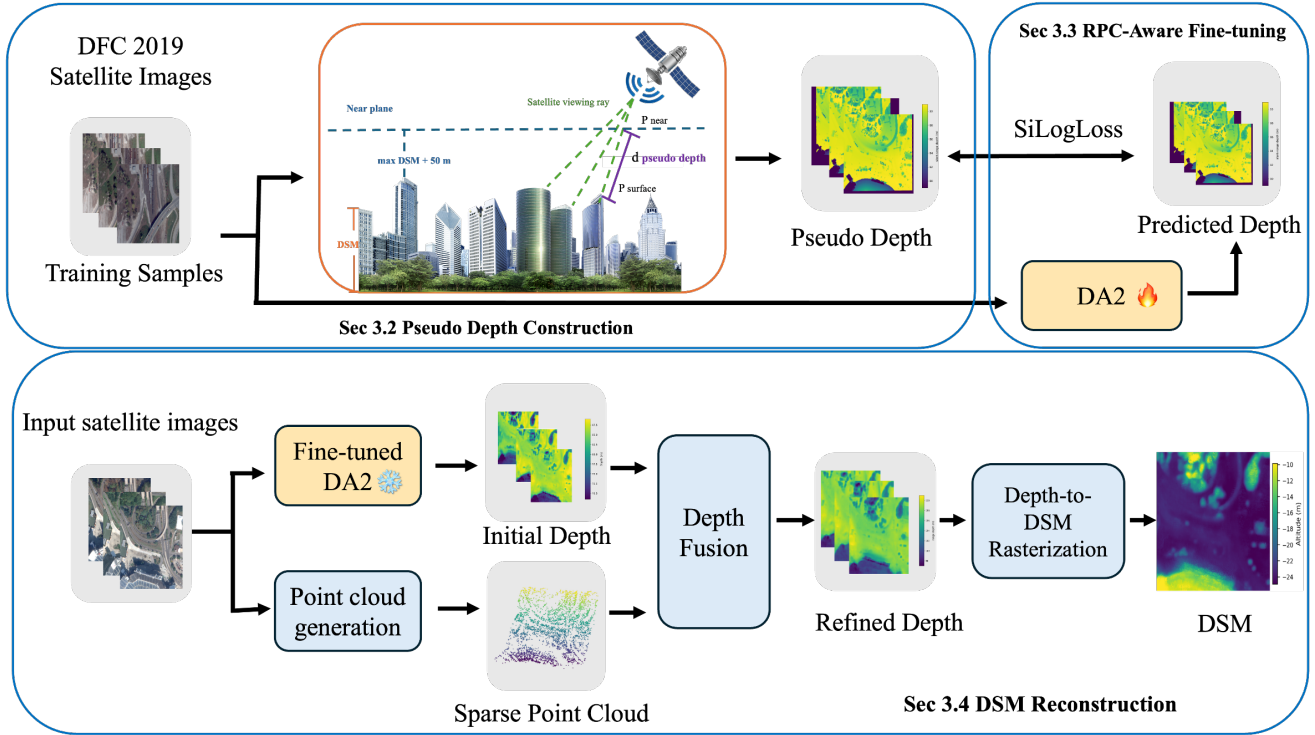


Figure 2. Overview of Sat3R. Given multi-view satellite images and their associated RPC models, we first construct pseudo depth supervision via slant-range geometry. The constructed image–depth pairs are used to fine-tune DA2 in an RPC-aware manner. At inference, per-view depth maps are fused and back-projected through the RPC model to produce the final DSM.

fixed-point iteration on the ground-truth DSM. The pseudo depth is then defined as the slant-range distance:

$$d = \|\mathbf{P}_{\text{surface}} - \mathbf{P}_{\text{near}}\|_2 \quad (2)$$

This construction provides per-pixel metric depth supervision for DA2 [28]. Training pairs are curated from DFC2019 [17] by retaining scenes with complete RGB–CLS alignment, sufficient multi-view coverage, and excluding winter scenes identified via IMD acquisition timestamps.

### 3.3. RPC-Aware Fine-tuning

We fine-tune DA2 [28] on the constructed image–depth pairs following the metric depth fine-tuning protocol of DA2, using the Scale-Invariant Logarithmic (SiLog) loss [1]:

$$\mathcal{L}_{\text{SiLog}} = \frac{1}{N} \sum_{i=1}^N (\log \hat{d}_i - \log d_i)^2 - \frac{\lambda}{N^2} \left( \sum_{i=1}^N \log \hat{d}_i - \log d_i \right)^2 \quad (3)$$

where  $\hat{d}_i$  and  $d_i$  are the predicted and pseudo ground-truth depth values respectively, and  $\lambda$  is a variance minimization factor. The maximum depth range for inference is set to 150 m to align with the satellite scene depth distribution. This enables Sat3R to directly output metric-scale depth without requiring scale recovery in post-processing.

### 3.4. DSM Reconstruction

At inference, DA2 predicts per-view depth maps with a maximum depth range of 150 m, calibrated to the satellite scene depth distribution. Per-view depth maps are fused into metric depth using the multi-view fusion module [8]. Each pixel’s fused depth  $d_i^*$  is back-projected into 3D space along its RPC imaging ray:

$$\mathbf{P}_i = \text{RPC}^{-1}(u_i, v_i, d_i^*) \quad (4)$$

where  $(u_i, v_i)$  is the image coordinate and  $\mathbf{P}_i \in \mathbb{R}^3$  is the recovered 3D point in geographic coordinates (longitude, latitude, altitude). The 3D points from all views are then aggregated and rasterized onto a uniform 2D grid, with height values pooled via p90 to produce the final DSM  $\mathbf{H} \in \mathbb{R}^{W \times H}$ . Since RPC-aware fine-tuning outputs metric-scale depth, it provides a better initial estimate for the fusion stage, accelerating convergence of the depth fusion optimization.

## 4. Experiments

### 4.1. Implementation Details

We train and evaluate on the DFC2019 satellite dataset [17]. Please refer to the appendix A for more details.

Method	JAX_207 MAE↓/MED↓	JAX_214 MAE↓/MED↓	JAX_260 MAE↓/MED↓	OMA_212 MAE↓/MED↓	OMA_287 MAE↓/MED↓	OMA_315 MAE↓/MED↓	Mean MAE↓/MED↓	Time↓
<i>Optimization-based methods</i>								
SatDN [8]	<b>2.399 / 1.214</b>	<b>1.816 / 0.732</b>	<b>1.620 / 0.961</b>	<u>0.888 / 0.529</u>	<b>0.894 / 0.405</b>	<b>1.022 / 0.598</b>	<b>1.44 / 0.74</b>	5h 36min
<i>Feed-forward methods</i>								
AnySplat [4]	4.477 / 3.743	8.689 / 6.665	4.897 / 4.138	1.123 / 1.938	3.153 / 2.247	2.930 / 2.201	4.21 / 3.49	1min 37s
VGGT [21]	5.519 / 4.476	6.346 / 4.121	3.699 / 2.711	2.786 / 2.234	3.804 / 2.509	2.483 / 1.647	4.11 / 2.95	1min 31s
DA3 [7]	4.647 / 3.653	8.341 / 5.651	4.658 / 5.651	2.118 / 1.193	3.557 / 2.816	2.887 / 2.058	4.37 / 3.50	1min 40s
DA2 [28]	4.578 / 3.254	7.841 / 5.403	4.014 / 3.224	4.230 / 3.078	3.681 / 3.203	3.214 / 2.486	4.59 / 3.44	<u>1min 26s</u>
<b>Ours</b>	<u>3.437 / 2.082</u>	<u>5.372 / 2.934</u>	<u>3.515 / 2.573</u>	<b>0.781 / 0.446</b>	<u>2.528 / 1.974</u>	<u>1.305 / 0.662</u>	<u>2.82 / 1.78</u>	<b>1min 05s</b>

Table 1. DSM reconstruction accuracy on six scenes from DFC2019 dataset [17]. Ours achieves the best performance among feed-forward methods and approaches optimization-based SatDN, while running over  $300\times$  faster.

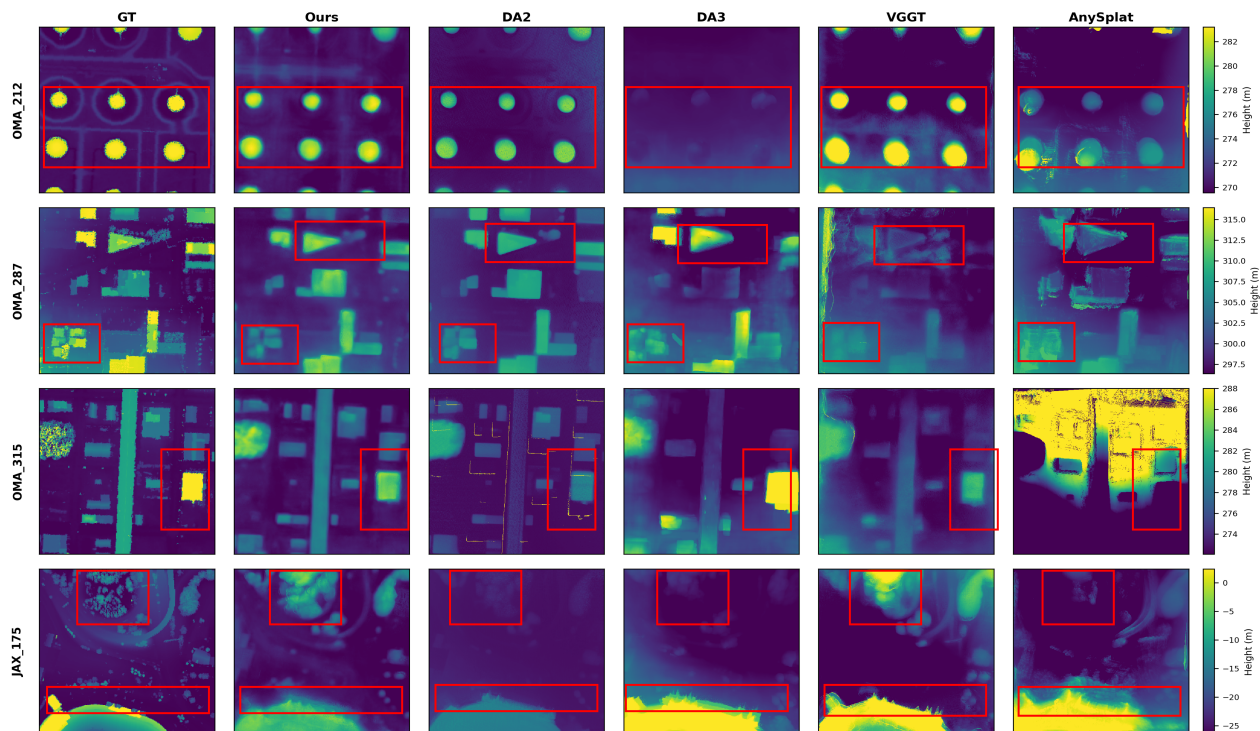


Figure 3. Qualitative comparison of DSM reconstruction results on selected DFC2019 scenes. Red boxes highlight representative regions where different methods show visible structural differences.

## 4.2. Experiment Results

As shown in Table 1, Sat3R consistently outperforms all feed-forward baselines, reducing mean MAE from 4.59 for zero-shot DA2 to 2.82 and mean MED from 3.44 to 1.78, demonstrating that RPC-aware metric depth fine-tuning effectively bridges the domain gap between natural and satellite imagery. Despite being a feed-forward method, Sat3R closely approaches the accuracy of the optimization-based upper bound SatDN, while delivering over  $300\times$  speedup.

As shown in Fig. 3, zero-shot feed-forward baselines suffer from severe scale drift and blurry boundaries due to the domain gap between natural and satellite imagery. In

contrast, Sat3R produces DSMs with accurate scale range, sharper building boundaries, and better preservation of fine-grained geometric details, closely matching the ground truth.

## 4.3. Ablation Study

We investigate the effect of the maximum depth threshold during inference. Detailed ablation results are provided in Appendix B.

## 5. Conclusion

We present Sat3R, a feed-forward framework for satellite DSM reconstruction that bridges the domain gap between natural and satellite imagery via RPC-aware fine-

tuning of Depth Anything V2. By constructing physically consistent pseudo depth supervision from RPC geometry, Sat3R adapts a monocular depth foundation model to the satellite domain without per-scene optimization. Experiments on DFC2019 [17] demonstrate that Sat3R achieves competitive accuracy against optimization-based methods while delivering over  $300\times$  speedup, establishing a practical and efficient baseline for satellite DSM reconstruction.

## References

- [1] Shariq Farooq Bhat, Reiner Birkel, Diana Wofk, Peter Wonka, and Matthias Müller. Zoedepth: Zero-shot transfer by combining relative and metric depth, 2023. 2, 3
- [2] Camille Billouard, Dawa Derksen, Emmanuelle Sarrazin, and Bruno Vallet. Sat-ngp : Unleashing neural graphics primitives for fast relightable transient-free 3d reconstruction from satellite imagery, 2024. 2
- [3] Binbin Huang, Zehao Yu, Anpei Chen, Andreas Geiger, and Shenghua Gao. 2d gaussian splatting for geometrically accurate radiance fields. In *SIGGRAPH 2024 Conference Papers*. Association for Computing Machinery, 2024. 2
- [4] Lihan Jiang, Yucheng Mao, Linning Xu, Tao Lu, Kerui Ren, Yichen Jin, Xudong Xu, Mulin Yu, Jiangmiao Pang, Feng Zhao, et al. Anysplat: Feed-forward 3d gaussian splatting from unconstrained views. *arXiv preprint arXiv:2505.23716*, 2025. 2, 4, 7
- [5] Bernhard Kerbl, Georgios Kopanas, Thomas Leimkühler, and George Drettakis. 3d gaussian splatting for real-time radiance field rendering. *ACM Transactions on Graphics*, 42(4), 2023. 2
- [6] Vincent Leroy, Johann Cabon, and Jerome Revaud. Grounding image matching in 3d with mast3r, 2024. 2
- [7] Haotong Lin, Sili Chen, Jun Hao Liew, Donny Y. Chen, Zhenyu Li, Guang Shi, Jiashi Feng, and Bingyi Kang. Depth anything 3: recovering the visual space from any views. *arXiv preprint arXiv:2511.10647*, 2025. 2, 4, 7
- [8] Tianle Liu, Shuangming Zhao, Wanshou Jiang, and Bingxuan Guo. Sat-dn: Implicit surface reconstruction from multi-view satellite images with depth and normal supervision. *arXiv preprint arXiv:2502.08352*, 2025. 1, 2, 3, 4, 7
- [9] Xi Liu, Chaoyi Zhou, and Siyu Huang. 3dgs-enhancer: Enhancing unbounded 3d gaussian splatting with view-consistent 2d diffusion priors. In *Advances in Neural Information Processing Systems (NeurIPS)*, 2024. 2
- [10] Roger Marí, Gabriele Facciolo, and Thibaud Ehret. Sat-NeRF: Learning multi-view satellite photogrammetry with transient objects and shadow modeling using RPC cameras. In *2022 IEEE/CVF Conference on Computer Vision and Pattern Recognition Workshops (CVPRW)*, pages 1310–1320, 2022. 2
- [11] Roger Marí, Gabriele Facciolo, and Thibaud Ehret. Multi-date earth observation nerf: The detail is in the shadows. In *Proceedings of the IEEE/CVF Conference on Computer Vision and Pattern Recognition (CVPR) Workshops*, pages 2034–2044, 2023. 2
- [12] Ben Mildenhall, Pratul P. Srinivasan, Matthew Tancik, Jonathan T. Barron, Ravi Ramamoorthi, and Ren Ng. Nerf: Representing scenes as neural radiance fields for view synthesis. In *ECCV*, 2020. 2
- [13] Ben Mildenhall, Dor Verbin, Pratul P. Srinivasan, Peter Hedman, Ricardo Martin-Brualla, and Jonathan T. Barron. MultiNeRF: A Code Release for Mip-NeRF 360, Ref-NeRF, and RawNeRF, 2022.
- [14] Thomas Müller, Alex Evans, Christoph Schied, and Alexander Keller. Instant neural graphics primitives with a multiresolution hash encoding. *ACM Trans. Graph.*, 41(4):102:1–102:15, 2022. 2
- [15] Linfei Pan, Daniel Barath, Marc Pollefeys, and Johannes Lutz Schönberger. Global Structure-from-Motion Revisited. In *European Conference on Computer Vision (ECCV)*, 2024. 2
- [16] Yingjie Qu and Fei Deng. Sat-mesh: Learning neural implicit surfaces for multi-view satellite reconstruction. *Remote Sensing*, 15:4297, 2023. 2
- [17] Bertrand Le Saux, Naoto Yokoya, Ronny Hänsch, and Myron Brown. Data fusion contest 2019 (dfc2019), 2019. 1, 2, 3, 4, 5
- [18] Johannes Lutz Schönberger and Jan-Michael Frahm. Structure-from-motion revisited. In *Conference on Computer Vision and Pattern Recognition (CVPR)*, 2016. 2
- [19] Johannes Lutz Schönberger, True Price, Torsten Sattler, Jan-Michael Frahm, and Marc Pollefeys. A vote-and-verify strategy for fast spatial verification in image retrieval. In *Asian Conference on Computer Vision (ACCV)*, 2016.
- [20] Johannes Lutz Schönberger, Enliang Zheng, Marc Pollefeys, and Jan-Michael Frahm. Pixelwise view selection for unstructured multi-view stereo. In *European Conference on Computer Vision (ECCV)*, 2016. 2
- [21] Jianyuan Wang, Minghao Chen, Nikita Karaev, Andrea Vedaldi, Christian Rupprecht, and David Novotny. Vggt: Visual geometry grounded transformer. In *Proceedings of the IEEE/CVF Conference on Computer Vision and Pattern Recognition*, 2025. 1, 2, 4, 7
- [22] Peng Wang, Lingjie Liu, Yuan Liu, Christian Theobalt, Taku Komura, and Wenping Wang. Neus: Learning neural implicit surfaces by volume rendering for multi-view reconstruction. *arXiv preprint arXiv:2106.10689*, 2021. 2
- [23] Qianqian Wang, Yifei Zhang, Aleksander Holynski, Alexei A Efros, and Angjoo Kanazawa. Continuous 3d perception model with persistent state. *arXiv preprint arXiv:2501.12387*, 2025. 2
- [24] Run Wang, Chaoyi Zhou, Amir Salarpour, Xi Liu, Zhi-Qi Cheng, Feng Luo, Mert D. Pesé, and Siyu Huang. Flexmap: Generalized hd map construction from flexible camera configurations, 2026.
- [25] Shuzhe Wang, Vincent Leroy, Johann Cabon, Boris Chidlovskii, and Jerome Revaud. Dust3r: Geometric 3d vision made easy. In *CVPR*, 2024.
- [26] Jianing Yang, Alexander Sax, Kevin J. Liang, Mikael Henaff, Hao Tang, Ang Cao, Joyce Chai, Franziska Meier, and Matt Feiszli. Fast3r: Towards 3d reconstruction of 1000+ images in one forward pass. In *Proceedings of the IEEE/CVF*

*Conference on Computer Vision and Pattern Recognition (CVPR)*, 2025. [2](#)

- [27] Lihe Yang, Bingyi Kang, Zilong Huang, Xiaogang Xu, Jiashi Feng, and Hengshuang Zhao. Depth anything: Unleashing the power of large-scale unlabeled data. In *CVPR*, 2024. [2](#)
- [28] Lihe Yang, Bingyi Kang, Zilong Huang, Zhen Zhao, Xiaogang Xu, Jiashi Feng, and Hengshuang Zhao. Depth anything v2. *arXiv:2406.09414*, 2024. [1](#), [2](#), [3](#), [4](#), [7](#)
- [29] Zehao Yu, Anpei Chen, Binbin Huang, Torsten Sattler, and Andreas Geiger. Mip-splatting: Alias-free 3d gaussian splatting. In *Proceedings of the IEEE/CVF Conference on Computer Vision and Pattern Recognition (CVPR)*, pages 19447–19456, 2024. [2](#)
- [30] Junyi Zhang, Charles Herrmann, Junhwa Hur, Varun Jampani, Trevor Darrell, Forrester Cole, Deqing Sun, and Ming-Hsuan Yang. Monst3r: A simple approach for estimating geometry in the presence of motion. *arXiv preprint arxiv:2410.03825*, 2024. [2](#)
- [31] Chaoyi Zhou, Xi Liu, Feng Luo, and Siyu Huang. Latent radiance fields with 3d-aware 2d representations. In *International Conference on Learning Representations (ICLR)*, 2025. [2](#)
- [32] Chaoyi Zhou, Run Wang, Feng Luo, Mert D. Pesé, Zhiwen Fan, Yiqi Zhong, and Siyu Huang. Ff3r: Feedforward feature 3d reconstruction from unconstrained views. In *CVPR Findings*, 2026. [2](#)

Max Depth	Mean MAE↓	Mean MED↓
100	3.312	2.254
300	3.412	2.354
<b>150</b>	<b>3.131</b>	<b>1.963</b>

Table 2. Ablation study on the maximum depth threshold.

## Appendix

In the Appendix, we provide the following:

- comprehensive implementation details in Section A
- comprehensive ablation details in Section B

### A. Implementation Details

Training pairs are constructed from scenes with complete RGB-CLS alignment and sufficient multi-view coverage, with winter scenes excluded via IMD acquisition timestamps. We fine-tune DA2 [28] for 40 epochs with a learning rate of  $5 \times 10^{-6}$  using the AdamW optimizer on  $2 \times$  NVIDIA A100 40GB GPUs. All inference experiments are conducted on a single NVIDIA A100 40GB GPU. At inference, per-view depth maps are fused using the SatDN fusion module [8] and rasterized to a DSM grid via p90 pooling. We evaluate on 6 held-out scenes (JAX\_207, JAX\_214, JAX\_260, OMA\_212, OMA\_287, OMA\_315) unseen during training, using Mean Absolute Error (MAE) and Median Error (MED) as metrics.

We compare against two categories of methods.

**Optimization-based:** SatDN [8], which fits a neural representation per scene and serves as the accuracy upper bound.

**Feed-forward:** DA2 [28], DA3 [7], VGGT [21], and AnySplat [4]. For all feed-forward baselines, per-view depths are processed through the same depth fusion, alignment, and rasterization pipeline to ensure a fair comparison.

### B. Ablation Study

As shown in Table 2 and Fig. 4, a threshold of 150m achieves the best performance across all metrics. A smaller value (100m) causes saturation near the depth boundary, while a larger value (300m) reduces effective depth resolution relative to the actual scene range ( $\sim 55$ – $94$  m), degrading accuracy. This confirms that aligning the depth range with the satellite data distribution is critical for effective fine-tuning.

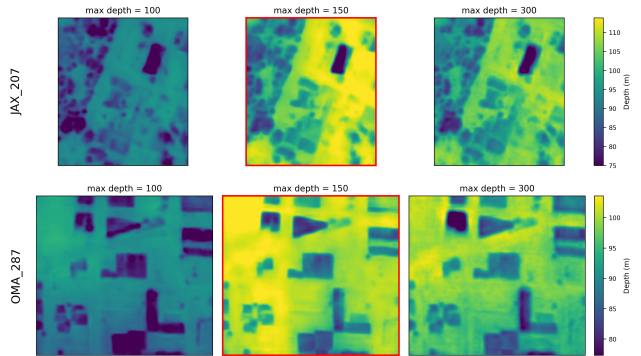


Figure 4. Qualitative ablation on the maximum depth threshold. Setting the threshold to 150m produces sharper boundaries and more accurate height estimation compared to 100m and 300m.